Cooperative Motion Control of Autonomous Marine Vehicles for Ocean Observation

Daniel Oluwatobi Akanji
Electrical and Computer Engineering
Instituto Superior Tecnico, Lisbon, Portugal
daniel.akanji@tecnico.ulisboa.pt

***Abstract*—Scientists employ diverse observing technologies and instruments to measure and monitor the global oceans. However, some, such as research vessels, are short-term and fall short in capturing long-term changes. Long-term ocean observations are vital for comprehending climate change, variability and improving climate, weather, and environmental hazard forecasting. This study presents a system that enables long-term observation through the use of Autonomous Marine Vehicles. The proposed robotic architecture consists of three mobile nodes: an Autonomous Surface Craft (ASC) and two Autonomous Underwater Vehicles (AUVs). The formation control strategy adopts a leader-follower approach; the ASC serves as a follower/tracker, while the AUVs act as leaders/targets. The ASC, equipped with sensors, gathers data at the air-sea interface and the ocean's upper column as it closely follows the AUVs. Conversely, the two AUVs make their observations as they dive through the water column at a given angle, following a predefined path in the horizontal plane while exhibiting a sawtooth-like motion in the vertical plane Path Following (PF) allows the target vehicles to follow a predefined path with the desired speed profile in the horizontal plane while controlling the pitch angle creates the motion in the vertical plane. Employing the Target Tracking approach, the tracker keeps adjusting its speed and orientation to the target to ensure close tracking. The final layer involves cooperative multiple-formation control, enabling synchronized movement with targets. Two cooperative formations are implemented: intermittent tracking of targets in the first, and tracking and following mid positions between targets in the second.**

***Index Terms*—Autonomous marine vehicle, Target Tracking, Cooperative multiple formation control, Path Following, Line of sight**

I. Introduction

In recent times, there has been an increase in the use of AMVs for various marine operations such as seafloor mapping, port protection, mine countermeasures, reconnaissance surveys, ocean observation and sampling, and surveillance missions. This system provides substantial advantages in terms of cost, data acquisition, and greater operational efficiency to traditional ocean exploration methods.

In ocean sampling and observation, the cost of traditional methods such as ships and their inability to stay out at sea for a long time has created interest in the use of autonomous robotic platforms such as autonomous surface crafts (ASCs) and autonomous underwater vehicles (AUVs). This paradigm shift is made possible due to advances in navigation sensors, low-power electronics, more efficient energy storage and advanced AI and control algorithms, amongst other factors [1].

There is a growing demand for improved observation capabilities, encompassing broader data coverage, longer durations, and refined measurement methods. Fulfilling these requirements is intricate and computationally demanding for an individual marine vehicle. Any malfunction in a sensor, actuator, or any component of the vehicle can disrupt such missions. Hence, an alternative solution embraced by researchers is the use of multiple marine vehicles that work in cooperation to meet those demands.

With the cooperation of multiple marine vehicles, significant mission characteristics, such as completion time, fault tolerance, cognition and perception of the augmented system, can be positively impacted [2]. A particularly important scenario that motivates the cooperation of multiple autonomous vehicles, and in a similar manner, poses a great challenge to system engineers, both from a theoretical and practical standpoint, is automatic ocean exploration/monitoring for scientific and commercial purposes. In this scenario, using a single vehicle can lead to system failure since the vehicle will be heavily equipped. However, cooperation between a group of vehicles connected via a mobile communications network has the potential to overcome this limitation [3].

The ongoing RAMONES (Radioactivity Monitoring in Ocean Ecosystems) project [4] serves as an inspiration for this effort, aiming to provide a novel solution for continuous in-situ ocean radioactivity monitoring. It involves three mobile nodes equipped with radiological instruments: an ASC, two AUGs, and a fixed benthic laboratory. Each node contributes to the mission's effectiveness by accomplishing specific tasks. This paper proposes a Guidance, Navigation, and Control approach to achieve cooperative control of a system capable of long-term ocean observation. The system consists of a surface vehicle and two underwater vehicles for collecting data both on the surface and at varying depths.

This paper is organized as follows: Section II presents a detailed description of the problem this project intends to address, Section III presents a brief review of the mathematical model of the AMVs and Section IV addresses the Path Following (PF) problem, with a comprehensive description of the algorithm applied to the problem at hand. In Section V, the Target Tracking problem was addressed with emphasis on the specific method used to solve the target tracking problem of the tracker vehicle, Section VI proposes the idea behind the cooperative formation of the vehicles in the network and finally Section VII presents the outcome of the study and some

recommendations for further studies.

II. Problem Definition

Consider two heterogeneous marine vehicles, where the first is a single ASC, and the second type is two AUVs. The end goal of the system is to have the ASC tracking and following the two AUVs, whose motion in the horizontal plane is following a predefined path and in the vertical plane performing a saw-tooth wave-like manoeuvre. The concept behind the design of this system is the leader-follower approach. In this approach, the two AUVs act as the leaders or targets while the ASC is the follower or tracker. In other words, for the surface vehicle to track the two AUVs, it can either track the mid position between the two vehicles or follow each target interchangeably. By choosing any of these formations, the ASC will be able to collect similar oceanographic data at the surface of the water column as the AUVs are doing below the water column. On the other end, the AUVs profile the water column as they perform their saw-tooth motion in the vertical plane and at the same time, traverse large distances as they follow a predefined path. With this system, data gathered will yield meaningful information about the changes both on a temporal and spatial scale, since they are collected below and at the surface of the water column simultaneously.

The technical aspect of the problem has been divided into sub-problems for simplicity's sake. The first problem to be solved is the Path Following problem. Path Following will ensure that the target vehicle follows a pre-defined path while tracking a path-dependent speed profile. Therefore, Path Following will characterise the motion of the two vehicles in the horizontal plane. Secondly, the problem of controlling the motion of the AUVs in that vertical plane will be addressed in order for the target vehicles to perform a saw-tooth wave-like motion in the vertical plane. The third problem is to ensure the tracker vehicle tracks and follows the target vehicles. To solve this problem, the Target Tracking approach will be employed such that the tracker will be required to track the targets either at midpoints or track them interchangeably. The tracker has access to the speed, attitude and position information of the targets in the formation. With the information received, the Target Tracking controller will ensure that the ASC always adjust its speed, and heading to be in line with the vehicle(s) it is tracking.

III. System Modelling

The notations and reference frames used in this paper are in keeping with the SNAME (Society of Naval and Marine Engineers) conventions. Generally, in robotics, two orthonormal coordinate frames are commonly used: the Earth-fixed inertial frame $\{\mathcal{I}\}$, composed of axes $x_{\mathcal{I}}$, $y_{\mathcal{I}}$, $z_{\mathcal{I}}$, and the body-fixed frame $\{B\}$, composed of the x_B, y_B, z_B axes, as shown in Fig. 1.

The rigid body kinematic equation is

$$\dot{\boldsymbol{\eta}} = \mathbf{R}(\psi)\boldsymbol{\nu}, \tag{1}$$

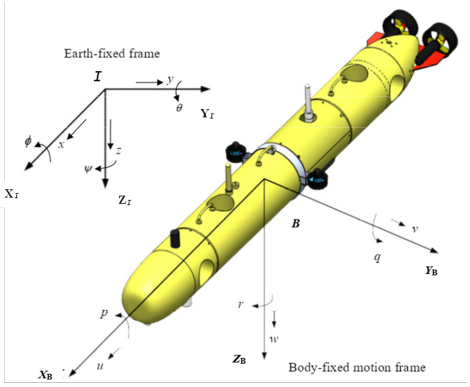

Fig. 1: Body-fixed and Inertial Reference frames [5]

where $\dot{\boldsymbol{\eta}}$ is the derivative of position with time, $\boldsymbol{\eta}$ = [x,y,ψ]^T represents the Earth-fixed position and heading angle, $\boldsymbol{\nu}$ = [u, v, r]^T represents the vessel-fixed velocities (surge, sway and yaw angular rate respectively) and $\boldsymbol{R}(\psi)$ is the rotation matrix from the Earth-fixed frame to the vessel-fixed frame. In this study, a simplified three-degree-of-freedom (3-DOF) vessel model is used to describe the ASC motions in the horizontal plane (i.e. surge, sway, and yaw) [6]. The roll, pitch, and heave are neglected. The simplified kinematic model can be written as

$$\begin{aligned} \dot{x} &= u\cos(\psi) - v\sin(\psi), \\ \dot{y} &= u\sin(\psi) + v\cos\psi, \\ \dot{\psi} &= r. \end{aligned} \tag{2}$$

For the underwater vehicle operating in the 3D plane, the 6-DOF equations of motions will be decomposed into a subsystem simple enough to capture the dynamics of the vehicle capable of solving the problem at hand. We assume that the sway (y), the roll angle (ϕ) and the heave z can be neglected, thereby reducing the control task to the surge (x), pitch (θ), and yaw (ψ). Following these assumptions, a simplified kinematic model can be written as

$$\begin{aligned} \dot{x} &= u\cos(\psi)\cos(\theta) - v\sin(\psi), \\ \dot{\theta} &= q, \\ \dot{\psi} &= r. \end{aligned} \tag{3}$$

The rigid-body dynamic equation can be written as

$$\boldsymbol{M}_{RB}\dot{\boldsymbol{\nu}} + \boldsymbol{C}_{RB}(\boldsymbol{\nu})\boldsymbol{\nu} = \boldsymbol{\tau}_{RB}, \tag{4}$$

where $\boldsymbol{M}_{RB}$ is the rigid-body mass matrix, C_{RB} is the rigid-body Coriolis and centripetal matrix due to the rotation of $\{B\}$ about the inertial frame $\{I\}$, ν = [u, v, w, p, q, r]^T is the generalized velocity vector expressed in $\{B\}$ and $\boldsymbol{\tau}_{RB}$ is a generalized vector of external forces and moments expressed in $\{B\}$. For the surface vehicle, the dynamic equation can be

written as

$$\begin{aligned} m_u\dot{u} - m_v vr + d_u u &= \tau_u, \\ m_v\dot{v} - m_u ur + d_v v &= 0, \\ m_r\dot{r} - m_{uv} uv + d_r r &= \tau_r, \end{aligned} \tag{5}$$

and the dynamics of the underwater vehicle can be written as

$$\begin{aligned} m_u\dot{u} + d_u u &= \tau_u, \\ m_q\dot{q} + d_q q + g &= \tau_q, \\ m_r\dot{r} + d_r r &= \tau_r, \end{aligned} \tag{6}$$

where m_u, m_v, m_q, m_r and m_{uv} represent the mass and hydrodynamic added mass and d_u, d_v, d_r, d_q, and d_r represent the hydrodynamic damping effects. τ_u is the external force in the x direction, the external torque about the Z-axis (differential mode) is τ_r, τ_q is the external torque about the Y-axis and g is the restoring force. From the (5) above, it can be seen that the τ_v is zero since the sway motion of a typical surface craft is not controllable.

IV. Path Following

Path Following (PF), is a core element of this cooperative motion system, integrated into the motion control system of target/leader vehicles. This renders it crucial. However, since Path Following is executed in the horizontal plane, an additional guidance motion will also be addressed in this section to achieve the saw-tooth motion in the vertical plane.

A. Path Following

The problem of PF entails making a vehicle converge to, and then follow a spatial path while asymptotically tracking the desired speed profile along the path. In PF, the vehicle is not required to be at specific positions at specific instants of time, unlike in trajectory tracking [7]. With this flexibility, PF has been known to yield a smoother convergence to the path and equally has reduced demands on the actuators of the vehicle, as compared to other guidance systems. One of this mission's characteristics is having vehicles that can perform long-term ocean observation. Therefore, the selected algorithm plays a vital role in the rate at which the vehicle's energy is expended. With less demanding actuation signals and consequent reduction of actuator movement, a substantial amount of energy can be conserved, thereby prolonging the overall mission time of the vehicles.

Various survey papers have presented diverse Path Following methods. However, Hung et al. [7] were able to classify various path-following algorithms into two categories based on the choice of the reference frame in which the path-following error was defined. In the first category, the methods stabilize the position error in the vehicle's body frame, as considered in [8] and [9], whereas, in the second category, the methods stabilize the position error in a frame attached to a reference point moving along the path, such as the Frenet-Serret (F-S) frame or the Parallel Transport (P-T) frame as presented in [10],[11]. The second approach is quite common as the popular Line of sight (LOS) algorithms follow the second convention. The PF method employed is the method presented by Lapierre et al. [12] where the PF error are stabilized in the path frame.

In addition to the SNAME notations, some notations particular to the PF problem will be explicitly stated. Let the symbol $\mathcal{I} = \{x_\mathcal{I}; y_\mathcal{I}\}$ denote an inertial (global) North-East (NE) frame, where the axis $x_\mathcal{I}$ points to the North and the axis $y_\mathcal{I}$ points to the East, Q be the center of mass of the vehicle and denote by $\mathbf{p} = [x; y] \in \mathbb{R}^2$ the position of Q in $\{\mathcal{I}\}$, and $\{B\} = \{\mathrm{x}_B, \mathrm{y}_B\}$ be a body-fixed frame whose origin is located at Q. In addition, denote by $\mathbf{v} = [u, v]^T \in \mathbb{R}^2$ the vehicle's velocity vector with respect to the fluid, measured in $\{B\}$, where u, v are the surge and sway speeds, respectively, $\mathcal{P}$ be the spatial path parametrized by a scalar variable γ. Denote by $\mathbf{p}_d$, the position of a generic point on the path in the inertial frame $\{\mathcal{I}\}$ described by the vector $\mathbf{p}_d = [x_d(\gamma), y_d(\gamma)]^T \in \mathbb{R}^2$ and $\mathbf{e}_\mathcal{P} \triangleq [s_1; y_1]^T \in \mathbb{R}^2$ be a vector defining the position error between the vehicle and the reference point $\mathbf{p}_d$, where s_1 and y_1 are called along-track and cross-track errors, respectively.

Given the 2-D spatial path $\mathcal{P}$ described by $\mathbf{p}_d = [x_d(\gamma), y_d(\gamma)]^T \in \mathbb{R}^2$, and a vehicle with the kinematics model described (3), derive a feedback control law for the vehicle's inputs (u and r) to fulfil the following tasks:

$i.$) ***Geometric task***: To steer the position error $\mathbf{e}_\mathcal{P} \triangleq \mathbf{p}$ - $\mathbf{p}_d$ such that

$$\lim_{t\to\infty} \mathbf{e}(t) = 0. \tag{7}$$

$ii.$) ***Dynamic task***: To ensure that the vehicle's forward speed u, tracks a positive desired speed profile U_d, i.e.,

$$\lim_{t\to\infty} u(t) - U_d(t) = 0. \tag{8}$$

Consider $u_\mathcal{P}$ to be the speed of the reference point P on the path with respect to the inertial frame, given by

$$u_\mathcal{P} = \frac{\mathrm{d}\mathbf{p}_d}{\mathrm{d}t} = \| \mathbf{p}_d'(\gamma) \| \dot{\gamma}, \tag{9}$$

where $\dot{\gamma}$ is the rate of evolution γ of the "reference point" along the path.

In what follows, we derive the dynamics of the PF errors between the vehicle and the path to achieve PF. The illustration in Fig. 2 shows the reference point $\mathbf{p}_d$ which the vehicle must track to achieve PF. Let $\{\mathcal{P}\}$ be the P-T frame attached to

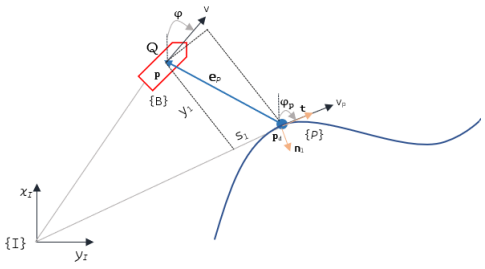

Fig. 2: Geometric illustration of Path Following Problem.

this point defined by rotating the inertial frame by angle $\psi_\mathcal{P}$, where $\psi_\mathcal{P}$ is the angle that the tangent vector at $\boldsymbol{p}_d$ makes

with $x_{\mathcal{I}}$ as seen in Fig. 2. With the position vector $\mathbf{e}_{\mathcal{P}}$ of the vehicle expressed in $\{\mathcal{P}\}$, it can be expressed mathematically as

$$\mathbf{e}_{\mathcal{P}} = \mathbf{R}_I^{\mathcal{P}}(\psi_{\mathcal{P}})(\mathbf{p} - \mathbf{p}_d), \tag{10}$$

where $\mathbf{R}_I^{\mathcal{P}} \in SO(2)$ is the rotation matrix from $\mathcal{I}$ to $\mathcal{P}$ defined as

$$\mathbf{R}_I^{\mathcal{P}}(\psi_{\mathcal{P}}) = \begin{bmatrix} \cos(\psi_{\mathcal{P}}) & \sin(\psi_{\mathcal{P}}) \\ -\sin(\psi_{\mathcal{P}}) & \cos(\psi_{\mathcal{P}}) \end{bmatrix}, \tag{11}$$

and

$$\begin{bmatrix} s_1 \\ y_1 \end{bmatrix} = \mathbf{R}_{\mathcal{I}}^{\mathcal{P}}(\psi_{\mathcal{P}}) \begin{bmatrix} x - x_p \\ y - y_p \end{bmatrix}. \tag{12}$$

Note that $\mathbf{R}_{\mathcal{I}}^{\mathcal{P}}(\psi_{\mathcal{P}}) = [\mathbf{R}_{\mathcal{P}}^{\mathcal{I}}(\psi_{\mathcal{P}})]^T$. Taking the time derivative of (10) to obtain a solution, we have

$$\dot{\mathbf{e}}_{\mathcal{P}} = [\dot{\mathbf{R}}_{\mathcal{P}}^{\mathcal{I}}(\psi_{\mathcal{P}})]^T(\mathbf{p} - \mathbf{p}_d) + \mathbf{R}_{\mathcal{I}}^{\mathcal{P}}(\psi_{\mathcal{P}})(\dot{\mathbf{p}} - \dot{\mathbf{p}}_d). \tag{13}$$

Following the proof in [6] (Rotation matrix differential equation, Theorem 2.2), let $\boldsymbol{R}_A^B \in SO(2)$ be the rotation matrix from {A} to frame {B}. Then,

$$\dot{\mathbf{R}}_A^B = \mathbf{R}_A^B \boldsymbol{S}(\omega_{A/B}^A), \tag{14}$$

where $\boldsymbol{S}(\omega_{A/B}^A)$ is the skew-symmetric matrix and $\omega_{A/B}^A \in \mathbb{R}^n$ is the angular velocity of {A} with respect to {B} expressed in {A}. Applying that to (13), it becomes

$$\dot{\mathbf{e}}_{\mathcal{P}} = -\boldsymbol{S}(\boldsymbol{\omega}_{\mathcal{P}})\mathbf{e}_{\mathcal{P}} + \mathbf{R}_{\mathcal{I}}^{\mathcal{P}}(\psi_{\mathcal{P}})\dot{\mathbf{p}} - \mathbf{R}_{\mathcal{I}}^{\mathcal{P}}(\psi_{\mathcal{P}})\dot{\mathbf{p}}_d, \tag{15}$$

where $\boldsymbol{S}(\boldsymbol{\omega}_{\mathcal{P}}) \in \mathbb{R}^{2\times 2}$ is a skew symmetric matrix parameterized by $\boldsymbol{\omega}_{\mathcal{P}} = [r_{\mathcal{P}},0]^T \in \mathbb{R}^2$, which is the angular velocity vector of $\{\mathcal{P}\}$ with respect to $\{\mathcal{I}\}$, expressed in $\{\mathcal{P}\}$. Note that $r_{\mathcal{P}}$ satisfies the relation

$$r_{\mathcal{P}} = k(\gamma)u_{\mathcal{P}}, \tag{16}$$

where $u_{\mathcal{P}}$ is the total speed of point *P* as shown in (9) and $k(\gamma)$ is the signed curvature of the path at P, given by

$$k(\gamma) = \frac{\dot{x}_d(\gamma)\ddot{y}_d(\gamma) - \ddot{x}_d(\gamma)\dot{y}_d(\gamma)}{||\dot{p}_d(\gamma)||^3}. \tag{17}$$

The proof of this can be found at the article on curvature [13] at Wolfram MathWorld. Note also that if γ is the arc length of the path then $||\dot{p}_d(\gamma)|| = 1$. In this case, $u_{\mathcal{P}} = \dot{\gamma}$, i.e. the speed of the "reference point" equals the rate of change of the path length.

Defining the orientation error ψ_e, between the vehicle's heading and the tangent of the path,

$$\psi_e \triangleq \psi - \psi_{\mathcal{P}}. \tag{18}$$

By expanding the second and the third part of (15), the following sets of equations are obtained

$$\mathbf{R}_{\mathcal{I}}^{\mathcal{P}}(\psi_{\mathcal{P}})\dot{\mathbf{p}} = \begin{bmatrix} u\cos(\psi_e) \\ u\sin(\psi_e) \end{bmatrix}, \tag{19}$$

$$\mathbf{R}_{\mathcal{I}}^{\mathcal{P}}(\psi_{\mathcal{P}})\dot{\mathbf{p}}_d = \mathbf{v}_{\mathcal{P}}, \tag{20}$$

where $\mathbf{v}_{\mathcal{P}} \triangleq [u_{\mathcal{P}}, 0\ ]^T \in \mathbb{R}^2$ is the velocity of $\mathbf{p}_d$ with respect to $\{\mathcal{I}\}$ expressed in $\{\mathcal{P}\}$. Substituting the expression in (19), (20) into (15), we obtain the dynamics of the position error as

$$\dot{\mathbf{e}} = -\boldsymbol{S}(\omega_{\mathcal{P}})\mathbf{e}_{\mathcal{P}} + \begin{bmatrix} u\cos(\psi_e) \\ u\sin(\psi_e) \end{bmatrix} - \begin{bmatrix} u_{\mathcal{P}} \\ 0 \end{bmatrix}, \tag{21}$$

and the dynamics of the orientation error is given by

$$\dot{\psi}_e = r - k(\gamma)u_{\mathcal{P}}. \tag{22}$$

Nonlinear Controller Design

Having derived the error dynamics, it is expedient to design the control laws that will drive the position and orientation error to zero. Writing (21) and (22) in a more compact form, we have

$$\begin{cases} \dot{s}_1 = r_{\mathcal{P}} y_1 + u\cos(\psi_e) - u_{\mathcal{P}}, \\ \dot{y}_1 = -r_{\mathcal{P}} s_1 + u\sin(\psi_e), \\ \dot{\psi} = r - k(\gamma)u_{\mathcal{P}}. \end{cases} \tag{23}$$

A Lyapunov candidate function (V_1) will be employed in deriving the required control laws. The function is given as

$$V_1 = \frac{1}{2}\mathbf{e}_{\mathcal{P}}^2 + \frac{1}{2k_2}(\tilde{\psi})^2, \tag{24}$$

where $\mathbf{e}_{\mathcal{P}}^2 = (s_1^2 + y_1^2)$, and

$$\tilde{\psi} = \psi_e - \delta(y_1, u). \tag{25}$$

$(s_1^2 + y_1^2)$ represents the distance between the vehicle and the path, which must converge to zero and $\delta(y_1, u)$ is a time-differentiable design function that can be used to shape the manner in which the vehicle approaches the path. The design of $\delta(y_1, u)$ must satisfy the following condition:

Condition IV.1. *:*

i.) $\delta(y_1, u) = 0,\ \forall_u,$
ii.) $y_1 \cdot u \cdot \sin(\delta(y_1, u)) \leqslant 0\ \forall_u, \forall_y.$

Taking its time derivative yields

$$\dot{V}_1 = \mathbf{e}_{\mathcal{P}}^T\dot{\mathbf{e}}_{\mathcal{P}} - \frac{1}{k_2}\tilde{\psi}\dot{\tilde{\psi}} \tag{26}$$

where $\dot{\tilde{\psi}} = r - k(\gamma)u_{\mathcal{P}} - \dot{\delta}$. Expanding and simplifying the equation yields

$$\begin{aligned} \dot{V}_1 &= s_1 \cdot \dot{s_1} + y_1 \cdot \dot{y_1} + \frac{1}{k_2}(\psi_e - \delta)(\dot{\psi_e} - \dot{\delta}) \\ &= s_1(r_{\mathcal{P}} y_1 + u \cdot \cos(\psi_e) - u_{\mathcal{P}}) + y_1(-r_{\mathcal{P}} s_1 + \\ &\quad u\sin(\psi_e)) + \frac{1}{k_2}(\psi_e - \delta)(\dot{\psi_e} - \dot{\delta}) \\ &= s_1(u\cos(\psi) - u_{\mathcal{P}}) + y_1 u\sin(\delta) + \frac{1}{k_2}(\psi_e - \delta)\Bigg(\dot{\psi_e} - \dot{\delta} \\ &\quad + k_2 \cdot y_1 \cdot u \cdot \frac{\sin(\psi_e) - \sin(\delta)}{\psi_e - \delta}\Bigg). \end{aligned} \tag{27}$$

We can now define the control laws

$$\begin{cases} u_{\mathcal{P}} = u\cos(\psi) + k_3 s_1, \\ \dot{\psi}_e = \dot{\delta} - k_2 \cdot y_1 \cdot u \cdot \frac{\sin(\psi_e)-\sin(\delta)}{\psi_e - \delta} - k_1(\psi_e - \delta), \end{cases} \tag{28}$$

where k_1, k_2 and k_3 are positive gains. Substituting (28) into (27), cancelling the undesirable terms, the derivative of the Lyapunov function becomes

$$\dot{V}_1 = -k_3 s_1^2 + y_1 u \sin(\delta) - \frac{k_1}{k_2}(\tilde{\psi})^2. \tag{29}$$

Note that from the second condition in IV.1, we conclude that $\dot{V}_1 \leqslant 0$ for all t. Furthermore, the above equation shows that $\dot{V}_1$ is uniformly continuous; thus, invoking Barbalat's lemma, $\dot{V}_1(t)$ converge to 0 as $t \to \infty$.

Therefore, the control law for u and r can be written as

$$u = U_d, \tag{30}$$

where U_d is the positive desired speed profile for the vehicle to track and

$$r = \kappa(\gamma) u_{\mathcal{P}} + \dot{\delta} - k_1(\tilde{\psi}) - k_2 y_1 u \frac{\sin(\psi_e) - \sin(\delta)}{\tilde{\psi}}, \tag{31}$$

where k_1, $k_2 > 0$ are tuning parameters, $\kappa(\gamma)$ is defined in 17, ψ_e and $\tilde{\psi}$ is given by (18 and 25) respectively, and $u_{\mathcal{P}}$ is given 28. Then, $\mathbf{e}_{\mathcal{P}}$(t), $\psi_e(t) \to 0$ as $t \to \infty$.

The control law for $u_{\mathcal{P}}$ in (28) implies that if the vehicle is behind/ahead of the "reference point" ($s_1 < 0 = s_1 > 0$) then the "reference point" decreases/increases its speed. This method excludes the vehicle from solving an optimization problem in order to find the closest point on the path to itself.

B. Vetical Motion System

To control the vertical motion of the vehicle, controlling the pitch angle of the vehicle will yield the desired motion in the vertical plane. Considering the kinematic model of the vehicle presented in (3), we assume that all other parameters except the pitch angle will be controlled. The glider vehicle performs optimally if moving in a yo-yo pattern, hence, the control law for the pitch angle θ is defined as

$$\begin{cases} z(t) \leqslant 1, & \theta(z) = -50^\circ, \\ z(t) \geqslant n, & \theta(z) = 50^\circ, \end{cases} \tag{32}$$

where z is the depth of the vehicle at time t and $n > 1$ is the maximum depth the vehicle will reach during the yo-yo maneuver. From the previous expression, it can be noted that the control law for the pitch is a function of the depth. For the vehicle to perform the required vertical manoeuvre as it follows its given path in the horizontal plane, the depth information of the vehicle is required for the pitch reference controller.

C. Simulations

1. Path Following: Fig. 3 shows the vehicle converges to the path and follows the path smoothly with a steady state error of $\pm 1.2m$. It is worth noting here that the vehicle was also performing the saw-tooth wave-like manoeuvre in the vertical plane while following a Lawn-mower path.

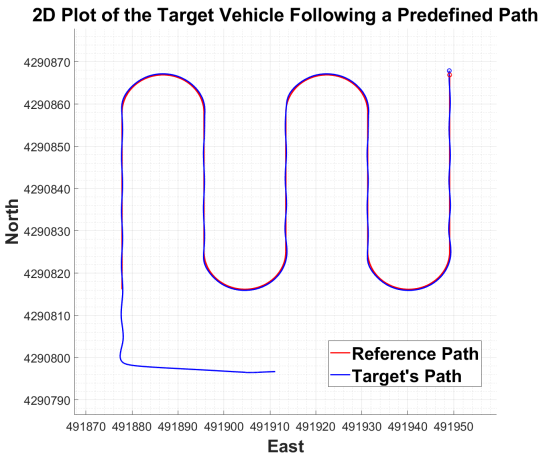

Fig. 3: Target vehicle following a lawn mower path in the horizontal plane.

2. Saw-tooth Wave-like Maneuver: Fig. 4 shows the vehicle moving up and down through the water column. It can be observed that the maximum depth of penetration as given in the simulation is 23m before it begins to resurface. It begins to dive back again as it reaches the surface at 1m. It maintains this cycle as it traverses its path in the horizontal plane.

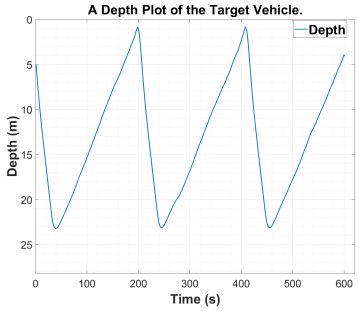

Fig. 4: Target vehicle performing a saw-tooth wave manoeuvre in the vertical plane.

3. Error Plot: One of the tools that can be employed to analyse the efficacy of a control algorithm is the error plot between the reference signal and the actual signal obtained. The position error between the vehicle and the predefined path can be seen in Fig. 5. The plot shows how the target vehicle converges with a distance of less than 1m between itself and the path.

4. Inner-loop References of the Target Vehicle: The three inner-loop references were responsible for driving the vehicle along the desired path. The surge plot with a constant reference speed of 0.3m/s demonstrates convergence to the signal despite perturbations. The surge plot perturbations relate to changes in the pitch reference signal. In the pitch plot, the vehicle seamlessly tracked its $\pm 50^\circ$ reference signal. Descending

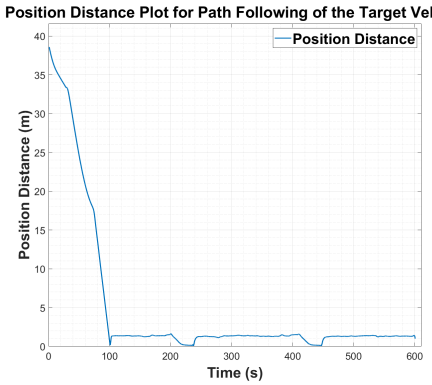

Fig. 5: Position Distance Error of Target Vehicle.

occurred at -50°, while ascending started at +50°. The pitch reference, despite having a similar magnitude but different direction, exhibits different performance in descending and ascending modes. The faster response in the descending mode can be attributed to the vehicle's lack of natural buoyancy. To stay at the surface during deployment, the vehicle relies on a stabilizer control system, which includes roll, pitch, and depth control, all set to 0 references. This explains why the vehicle descends faster than it ascends. The yaw plot illustrated the vehicle's tracking of the reference heading provided by the PF controller.

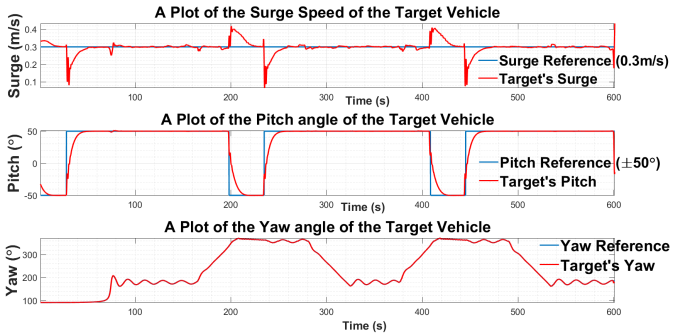

Fig. 6: Surge, Pitch and Yaw of Target Vehicle.

V. Tracker Tracking

In the context of guidance navigation and control, target tracking refers to the process by which the information received from sensor measurements is used to estimate the state of the target object, such as the target's position, velocity, and orientation. This information is then used to guide and control the tracker vehicle towards the target [14]. In target tracking, information about the path or trajectory and the future motion of the target is unknown. Hence, with only information about the present state of the target, guidance laws can be designed for the tracker/interceptor to track/intercept the target.

Consider the 2D position of the target denoted by $\mathbf{p}_d = [x_d, y_d]^T$ and let the position of the tracker vehicle be denoted by $\mathbf{p} = [x, y]^T \in \mathbb{R}^2$, the control objective of a target-tracking scenario can be stated as

$$\lim_{t\to\infty} \left[\mathbf{p}(t) - \mathbf{p}_d(t)\right] = 0, \tag{33}$$

where $\mathbf{p}_d(t)$ is moving by a (non-zero and bounded) velocity $\mathbf{v}_d(t) \triangleq \dot{\mathbf{p}}_d(t) \in \mathbb{R}^2$.

To achieve this control objective, control laws for the tracker's speed and heading are designed to guide the tracker to the target.

A. Target Tracking Heading Controller

The widely used Line of Sight (LOS) algorithm will guide the design of a heading controller. This algorithm's core idea is that the tracker vehicle should consistently adjust its velocity to a look-ahead distance of the target vehicle, ensuring synchronization and catch-up. This approach eliminates the need for the tracker to reverse direction if ahead of the target; instead, it projects the target's position along its (target) longitudinal axis. Similarly, if behind the target, it maintains velocity toward the look-ahead distance. This assumption simplifies LOS into a straight-line problem, making it easier to solve.

Steering Law for Straight Lines

Consider an imaginary straight-line path implicitly defined by two waypoints; $\mathbf{p}_d \triangleq [x_d, y_d]^T \in \mathbb{R}^2$ and $\mathbf{p}_{d+\delta} \triangleq [x_{d+\delta}, y_{d+\delta}]^T \in \mathbb{R}^2$ respectively. $\mathbf{p}_d$ represents the position of the target along a predefined path and $\mathbf{p}_{d+\delta}$ is the projection of the target position $\mathbf{p}_d$ by an arbitrary distance δ along the targets longitudinal axis. Also, consider a body-fixed frame with origin at $\mathbf{p}_d$, whose whose x-axis has been rotated a positive angle $\psi_d \triangleq \text{atan2}(y_{d+\delta} - y_d, x_{d+\delta} - x_d) \in \mathbb{S}$ relative to the x-axis of the stationary reference frame $\{\mathcal{I}\}$ as illustrated in Fig. 7. Hence, the coordinates of the kinematic vehicle in

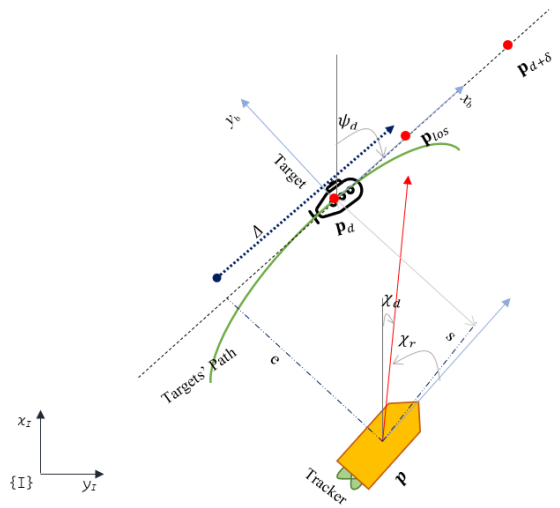

Fig. 7: An Illustration of the Straight Line Problem for Target Tracking.

the body-fixed frame of the target can be computed by

$$\varepsilon(t) = \mathbf{R}_{\mathcal{I}}^{\mathcal{B}}(\psi)^T(\mathbf{p}(t) - \mathbf{p}_(t)), \tag{34}$$

where $\mathbf{R}_I^{\mathcal{B}}$ is the rotation matrix from $\mathcal{I}$ to $\mathcal{B}$ defined as

$$\mathbf{R}_{\mathcal{I}}^{\mathcal{B}}(\psi) = \begin{bmatrix} \cos(\psi) & -\sin(\psi) \\ \sin(\psi) & \cos(\psi) \end{bmatrix}, \tag{35}$$

and $\varepsilon(t) \triangleq [s(t), e(t)]^T \in \mathbb{R}^2$ consists of the along-track distance s(t) and the cross-track error e(t) as shown in Fig. 7. The expression in (34) can be written as

$$\begin{bmatrix} s(t) \\ e(t) \end{bmatrix} = \mathbf{R}_{\mathcal{I}}^{\mathcal{B}}(\psi) \begin{bmatrix} x - x_d \\ y - y_d \end{bmatrix}. \tag{36}$$

Expanding (36), the cross-track error and the along-track error can be explicitly stated by

$$e(t) = -\big(x(t) - x_d\big)\sin(\psi) + \big(y(t) - y_d\big)\cos(\psi) \tag{37}$$

and

$$s(t) = \big(x(t) - x_d\big)\cos(\psi) + \big(y(t) - y_d\big)\sin(\psi) \tag{38}$$

respectively. The overall control objective remains the same as presented in (33). However, since the task is viewed as a straight-line problem, only the cross-track error becomes relevant such that e(t) = 0, means that the tracker has converged to the straight line along the longitudinal axis of the target. The along-track error between the tracker and the target is also important and therefore, the target tracking speed controller that will be discussed in the next section will cater for that.

The control objective associated with this straight-line problem becomes

$$\lim_{t\to\infty} e(t) = 0. \tag{39}$$

The lookahead-Based approach involves determining the desired course angle χ using an auxiliary lookahead distance that defines the $\mathbf{p}_{los}$, the intersection point of the LOS on the path. Since the position of the target $\mathbf{p}_d$ is known, the lookahead distance is employed to locate $\mathbf{p}_{los}$ further along the imaginary straight-line path from the target. For the Lookahead-based steering, the desired course angle χ is assigned by two components

$$\chi(e) = \chi_d + \chi_r(e), \tag{40}$$

where $\chi_d = \psi_d$ is equivalent to the heading angle of the target vehicle, while

$$\chi_r(e) = \arctan\Big(\frac{-e}{\Delta}\Big) \quad = \arctan(-K_p e), \tag{41}$$

is a velocity-path relative angle, which ensures that the velocity is directed toward a point on the path that is located at a lookahead distance $\Delta(t) > 0$. This feature can be quite useful since the angle is always restricted between $\chi_r(e) \in [-\pi/2, \pi/2]$.In what follows, $K_p = 1/\Delta > 0$ and works like proportional gain. (40) can be written as

$$\chi(e) = \psi_d + \arctan\Big(\frac{-e}{\Delta}\Big). \tag{42}$$

B. Target Tracking Speed Controller

Following the intuition presented in Section V-A such that the tracker vehicle should move side by side with the target vehicle, the speed control law will be responsible for regulating its speed to meet up when it is behind the target or to slow down for the target vehicle if it is ahead at any time. With this strategy, whenever the tracker catches up with the target, it will move at the same speed as the target.

Consider the Lyapunov function candidate

$$V_2 = \frac{1}{2}(s^2 + e^2), \quad s \neq 0, e \neq 0. \tag{43}$$

The desired approach angle ψ_d is the function of the cross-track error (e) as given in (42). The error coordinates for control design purposes for s, e and $\tilde{\psi}_e = \psi_d - \psi$ between the target and tracker should be driven to zero. $\tilde{\psi}_e = \chi_r = \arctan(-e/\Delta)$ as given in (42).

The time derivative of V_2 under the assumption that $\tilde{\psi}_e = \chi_r$ is

$$\begin{aligned} \dot{V}_2 &= s \cdot \dot{s} + e \cdot \dot{e} \\ &= s\Big(r_B e + u - u_d\cos(\tilde{\psi}_e)\Big) + e\Big(-r_B s + u_d \sin(\tilde{\psi}_e)\Big) \\ &= s\Big(u - u_d\cos(\tilde{\psi}_e)\Big) + eu\sin(\tilde{\psi}_e), \end{aligned} \tag{44}$$

where r_B is the angular velocity of the $\{B\}$ of the target with respect to $\{\mathcal{I}\}$ expressed in its $\{B\}$ obtained from the skew symmetric matrix given in (14), u is the speed of the tracker with respect to $\{\mathcal{I}\}$ and u_d is the speed of the target. We can now define the control law

$$\Big\{u = u_d\cos(\tilde{\psi}_e) - k_3 s. \tag{45}$$

where $k_3 > 0$ is the positive gain. Substituting (45) into (44), cancelling the undesirable terms, the derivative of the Lyapunov function becomes

$$\dot{V}_2 = -k_3 s^2 + e u_d \sin(\tilde{\psi}_e). \tag{46}$$

Exploiting the fact that χ_r given by (41) satisfies

$$\sin(\tilde{\psi}_e) = \frac{-e}{\sqrt{e^2 + \Delta^2}}, \tag{47}$$

then the derivative of the Lyapunov V_2 can be written as

$$\dot{V}_2 = -k_3 s^2 - \frac{u_d}{\sqrt{e^2 + \Delta^2}} e^2 < 0, \quad s \neq 0, e \neq 0, \tag{48}$$

for $u_>0$ and $\Delta > 0$. We can conclude that $\dot{V}_2 \leqslant 0$ for all t. Since the Lyapunov function is positive definite and radially unbounded, while its derivative with respect to time is negative, standard Lyapunov arguments for the system prove that the equilibrium point $(s, e, \tilde{\psi}_e)$ = (0,0,0) is uniform global asymptotical stable (UGAS). These control laws ensure that the position and orientation of the tracker converge to that of

the target in a finite time.

Note that for a positive along-track error i.e., the tracker is ahead of the vehicle, the controller outputs a negative relative speed reference (with respect to the target); and vice versa for a negative along-track error. However, since we do not want the tracker vehicle to move backwards during the mission (i.e., with the negative relative speed), and at the same time, we do not also want the reference speed that will be generated by this controller to be above the maximum speed limit of the tracker vehicle, a saturation command will be introduced to the control law. This saturation command will ensure that the control law output does not yield negative speed and that the maximum reference speed will not exceed the maximum speed limit of the tracker vehicle. Hence, the saturation command can be written as

$$u_{sat} = Sat(u) := \begin{cases} u_{sat} = 0.05, & u \leqslant 0, \\ u_{sat} = 1.5, & u > 1.5, \\ u_{sat} = u_d \cos(\psi_e) + k_3 s, & \text{otherwise.} \end{cases} \tag{49}$$

C. Simulations

1. Tracker Following the Target Vehicle: Fig. 8 presents the result, which shows how well the tracker vehicle was able to stay on the target vehicle. It can be seen that the tracker's

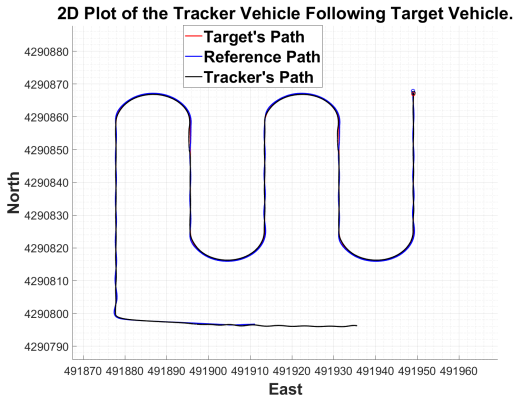

Fig. 8: 2D plot of the tracker following the target vehicle

path followed the target intimately with a steady state error of $\approx 1m$.

2. Error Plot: The along-track error in Fig. 9 shows that the tracker followed the target seamlessly. As the tracker began to converge to the target's position, there was an overshoot as seen in the plot, however, it can be seen that the tracker had to slow down for the target vehicle to catch up resulting in the sharp-peaked point on the plot.

3. Inner-Loop References of the Target and Tracker Vehicles: Fig. 10 displays the surge and yaw plots of the target and tracker vehicles. The tracker closely follows the target, as seen in the error plots from Fig. 9. Although the tracker's speed slightly exceeds the target's due to a simpler manoeuvre

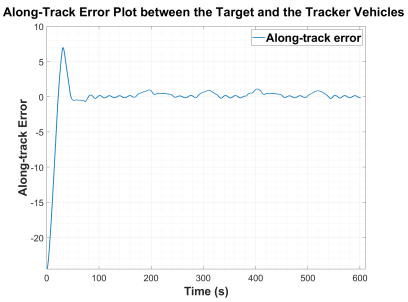

Fig. 9: Along-track error between the Target vehicle and the Tracker Vehicle

(horizontal motion) it undertook as compared to the target (yo-yo motion) thereby resulting in increased thruster performance for the tracker, its speed, however, is similar to that of the target. Additionally, the yaw plot demonstrates the tracker's heading aligning with the target's, influenced by the outer-loop PF controller's supplied reference.

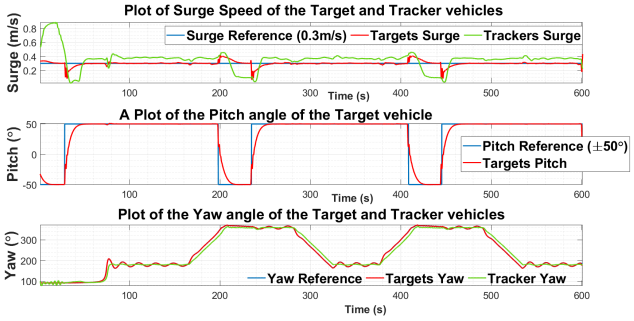

Fig. 10: Surge, Pitch and Yaw References of the tracker and target vehicles

VI. Cooperative Multiple Vehicle Formation Control

In a general context, cooperation among autonomous vehicles—whether they're marine, ground, or aerial—establishes a system where the movement of one or more vehicles in a formation relies on others. Sometimes, their movements are mutually dependent. To achieve this, effective communication with the relevant vehicles is essential. In this study, we assume there is continuous communication and the focus is on utilizing the information acquired in the network, rather than its acquisition process. Fig. 11 depicts the vehicle topology network, with nodes 1 and 2 representing the two AUVs, and node 0 corresponding to the ASC.

From the communication topology, the only vehicle that uses the information in the network is the surface craft while the motion of the two AUVs are independent. The question now becomes how it uses the information to follow the vehicles in the network. To answer this question, we present two approaches in which the surface craft can move in cooperation with the two underwater vehicles.

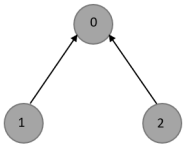

Fig. 11: A Directed Graph of the Vehicle Network Topology.

Scenario I

In this approach, the ASC is expected to follow the two AUVs intermittently such that it follows one at a time and later switches to the other. To achieve this a time function will be introduced such that the switching of which vehicle it follows will be dependent on the time function. Let the Target Tracking task be TgT, such that the tracker vehicle tracks one vehicle (vh_n) at the time (t) where n is the vehicle's ID. These can be written as

$$\text{Tgt}\Big(t(vh_n)\Big) = \begin{cases} t \in [0, t_{drt}], & \text{track AUV}_1, \\ t \in [t_{drt}, t_{drt} * 2], & \text{track AUV}_2, \\ t \in [t_{drt} * 2, t_{drt} * 3], & \text{track AUV}_1, \\ t \in [t_{drt} * 3, t_{drt} * 4], & \text{track AUV}_2, \\ \dots \end{cases} \tag{50}$$

where the drt is the duration for tracking each vehicle. After following a vehicle for a given duration, it switches to track the other vehicle, and this cycle continues. A description of this scenario can be seen in Fig. 12.

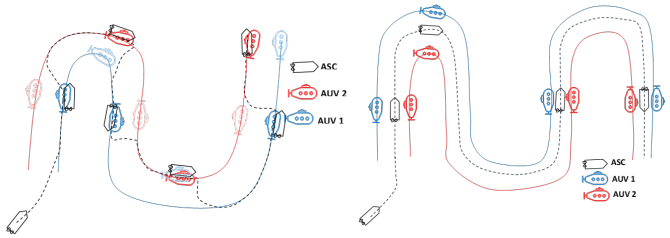

Fig. 12: Two Cooperation Strategies

Scenario II

Unlike the first, this approach does not need to switch between the vehicles. This scenario is the most common type of cooperation, in which the vehicle will have to move in synchrony as one single unit. For this formation, the tracker vehicle will have to estimate the mid position between the two AUVs and then track these points as some sort of virtual target. With this formation, the data measured by the surface craft will represent what takes place at the surface, above the area the underwater vehicles are observing. An estimation of the midpoint can be written as

$$\text{TgT} = \frac{1}{2}(\mathbf{p}_{auv1} + \mathbf{p}_{auv2}), \tag{51}$$

where $\mathbf{p}_{auv1}$ and $\mathbf{p}_{auv2}$ are the position vectors of AUV 1 & 2 respectively which are the projection of the average AUV positions into 2D, e.g. (x,y,0)and TgT is the Target Tracking task. A typical illustration of this approach can be seen in Fig. 12.

A. Control Block Representation

An illustration of the cooperative system is presented in Fig. 13 below. This block diagram sums up the entire system.

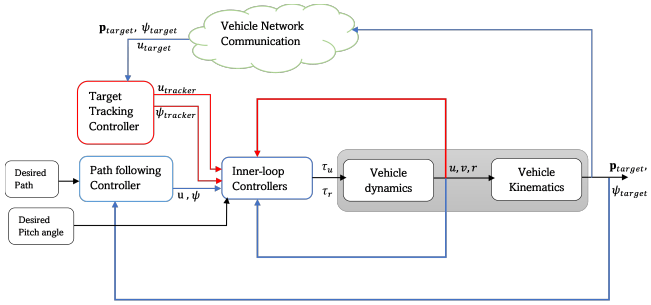

Fig. 13: Cooperative Control Block Diagram.

B. Simulations

1. Scenario I

Fig. 14 shows the tracker vehicle with the black coloured path intermittently following the targets with the blue and green paths. Each of the targets is independently following a lawn mower path. The condition for tracking each target is after every 240sec. Furthermore, it can be seen from the plot how the tracker vehicle smoothly transitions from one target to another and vice versa.

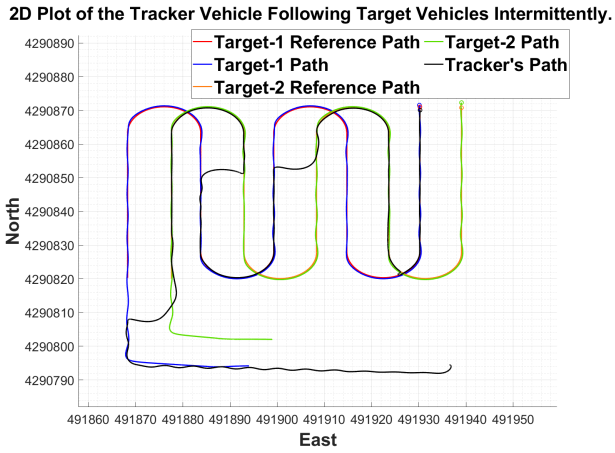

Fig. 14: 2D plot of the tracker following the target vehicles Intermittently

2. Scenario II

In this second configuration, the tracker vehicle tracks the mid position between the two targets as seen in Fig. 15.

VII. Conclusion

In conclusion, this study addressed cooperative control for heterogeneous vehicles in ocean observation. It applied concepts like Path Following and Target Tracking from guidance

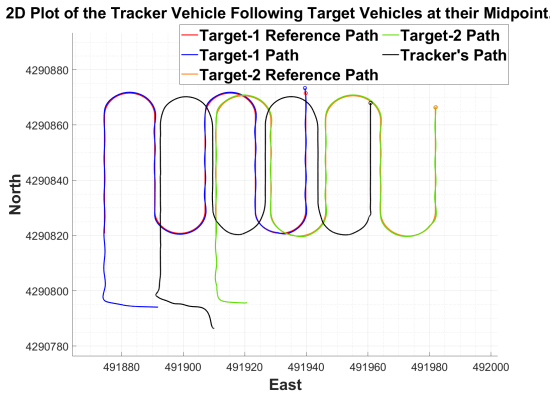

Fig. 15: 2D plot of the tracker following the target vehicles Intermittently

navigation and control. The system included two AUVs and an ASC, with the ASC moving at the surface in sync with the AUVs. The AUVs executed a saw-tooth manoeuvre vertically while following a predefined path horizontally. For cooperative formation control, two strategies were introduced: one involving intermittent tracking of individual targets and the other estimating and following the mid-position between targets. Comparing the formations in the light of ocean observation, the second formation seemed preferable for comprehensive data. Future work includes solving navigation issues, accounting for environmental disturbances, and using optimization/AI-based methods for formation decisions.

Acknowledgment

Many thanks to my supervisors, Prof. Pedro Batista and Prof. David Cabecinhas, for their guidance and advice towards the success of this scientific piece. I also acknowledge the European Regional Development Fund (FEDER), which funded my research through the Lisbon Regional Operational Program 2020 (LISBOA-01-0145-FEDER-022157), within the scope of the project (1018P.05390.1.01) EMSO-PT-PINFRA/22157/2016_LISBOA-01-01 alongside the RAMONES project (H2020 EU project RAMONES - Radioactivity Monitoring in Ocean Ecosystems, g.a. 101017808).

References

1 Nuno Cruz. *Adaptive Ocean Sampling with Modular Robotic Platforms*. PhD thesis, 04 2016.

2 Charalampos P. Bechlioulis, Fotis Giagkas, George C. Karras, and Kostas J. Kyriakopoulos. Robust formation control for multiple underwater vehicles. *Frontiers in Robotics and AI*, 6, 2019.

3 A. Pedro Aguiar, J. Almeida, M. Bayat, B. Cardeira, R. Cunha, A. Häusler, P. Maurya, A. Oliveira, A. Pascoal, A. Pereira, M. Rufino, L. SebastiÃo, C. Silvestre, and F. Vanni. Cooperative control of multiple marine vehicles theoretical challenges and practical issues. *IFAC Proceedings Volumes*, 42(18):412–417, 2009. 8th IFAC Conference on Manoeuvring and Control of Marine Craft.

4 T. J. Mertzimekis, P. Nomikou, E. Petra, P. Batista, D. Cabecinhas, A. Pascoal, L. Sebastiño, J. Escartín, K. Kebkal, K. Karantzalos, A. Mallios, K. Nikolopoulos, and L. Maigne. The eu project ramones – continuous, long-term autonomous monitoring of underwater radioactivity. In *Atas das 7.as Jornadas de Engenharia Hidrográfica / 2. as Jornadas Luso-Espanholas de Hidrografia*, page 351–354. Instituto Hidrográfico, 2022, June 2022.

5 Guofang Chen, Yihui Liu, Ziyang Zhang, and Yufei Xu. Adaptive disturbance-observer-based continuous sliding mode control for small autonomous underwater vehicles in the trans-atlantic geotraverse hydrothermal field with trajectory modeling based on the path. *Journal of Marine Science and Engineering*, 10:721, 05 2022.

6 Thor I. Fossen. *Handbook of Marine Craft Hydrodynamics and Motion Control:Guidance Systems*, chapter 10, pages 241–284. John Wiley Sons, Ltd, 2011.

7 Nguyen Hung, Francisco Rego, Joao Quintas, Joao Cruz, Marcelo Jacinto, David Souto, Andre Potes, Luis Sebastiao, and Antonio Pascoal. A review of path following control strategies for autonomous robotic vehicles: Theory, simulations, and experiments. *Journal of Field Robotics*, 40(3):747–779, 2023.

8 Antonio Pedro Aguiar and João Pedro Hespanha. Trajectory-tracking and path-following of underactuated autonomous vehicles with parametric modeling uncertainty. *IEEE Transactions on Automatic Control*, 52:1362–1379, 2007.

9 Andrea Alessandretti, A. Pedro Aguiar, and Colin Jones. Trajectory-tracking and path-following controllers for constrained underactuated vehicles using model predictive control. *2013 European Control Conference, ECC 2013*, pages 1371–1376, 07 2013. 10.23919/ECC.2013.6669717.

10 Fotis A. Papoulias. Bifurcation analysis of line of sight vehicle guidance using sliding modes. *International Journal of Bifurcation and Chaos*, 01:849–865, 1991.

11 Nguyen T. Hung, F. Rego, N. Crasta, and A.M. Pascoal. Input-constrained path following for autonomous marine vehicles with a global region of attraction. *IFAC-PapersOnLine*, 51(29):348–353, 2018. 11th IFAC Conference on Control Applications in Marine Systems, Robotics, and Vehicles CAMS 2018.

12 Lionel Lapierre, Didik Soetanto, and António Manuel Santos Pascoal. Nonlinear path following with applications to the control of autonomous underwater vehicles. *42nd IEEE International Conference on Decision and Control (IEEE Cat. No.03CH37475)*, 2:1256–1261 Vol.2, 2003.

13 Weisstein Eric W. Curvature and normal vectors of a curve. https://mathworld.wolfram.com/Curvature.html, 2023.

14 Manav Kumar and Sharifuddin Mondal. Recent developments on target tracking problems: A review. *Ocean Engineering*, 236:109558, 2021. https://www.sciencedirect.com/science/article/pii/S0029801821009471.